Silica-Coated SPIONs Induce Ferroptosis in Endothelial Cells While Oleic Acid Mitigates Their Cytotoxic Effects

Neža Repar, Saša Kupčič, Sara Michelini, Eva Jarc Jovičić, Ana Kump, Matej Hočevar, Slavko Kralj, Toni Petan & Damjana Drobne

Published online: 20 Dec 2025.

Submit your article to this journal ⬚

Article views: 56

View related articles ⬚

View Crossmark data ⬚

Dovepress
Taylor & Francis Group

ORIGINAL RESEARCH

Silica-Coated SPIONs Induce Ferroptosis in Endothelial Cells While Oleic Acid Mitigates Their Cytotoxic Effects

Neža Repar[1], Saša Kupčič[1], Sara Michelini [1], Eva Jarc Jovičić [2], Ana Kump[2,3], Matej Hočevar [4], Slavko Kralj [5,6], Toni Petan [2], Damjana Drobne [1]

[1]Department of Biology, Biotechnical Faculty, University of Ljubljana, Ljubljana, Slovenia; [2]Department of Molecular and Biomedical Sciences, Jožef Stefan Institute, Ljubljana, Slovenia; [3]Jožef Stefan International Postgraduate School, Ljubljana, Slovenia; [4]Department of Physics and Chemistry of Materials, Institute of Metals and Technology (IMT), Ljubljana, Slovenia; [5]Department for Materials Synthesis, Jožef Stefan Institute, Ljubljana, Slovenia; [6]Department of Pharmaceutical Technology, Faculty of Pharmacy, University of Ljubljana, Ljubljana, Slovenia

Correspondence: Damjana Drobne, Biotechnical Faculty, Department of Biology, University of Ljubljana, Jamnikarjeva ulica 101, Ljubljana, 1000, Slovenia, Email damjana.drobne@bf.uni-lj.si

Purpose: Induction of ferroptosis, a form of cell death driven by iron-dependent lipid peroxidation, holds promise as a novel cancer therapy. Superparamagnetic iron oxide nanoparticles (SPIONs) have been proven able to induce ferroptosis in tumour cells, while their effects on non-cancerous cells remain unclear. In this study, we investigated the ability of silica-coated SPIONs to induce ferroptosis in human umbilical vein endothelial cells (HUVEC) and explored the potential protective effects of oleic acid (OA). Additionally, we evaluated the applicability of scanning electron microscopy (SEM) in distinguishing between ferroptotic and apoptotic cell death.
Results: We confirmed that silica-coated SPIONs, (used at concentrations of 25 and 50 µg/mL) increased lipid peroxidation and ROS formation in a dose-dependent manner up to 4.9- and 4-fold compared to controls, ultimately promoting ferroptosis without evidence of apoptosis, as indicated by the absence of phosphatidylserine-positive, propidium iodide-negative cells in flow cytometry experiments. Consistent with these results, the ferroptosis inhibitors α-tocopherol and ferrostatin-1 attenuated SPION-induced cytotoxicity, supporting ferroptosis as the primary mechanism of cell death. OA also protected cells from SPION-induced cytotoxicity by reducing lipid peroxidation, ROS formation, and cell death (from 58% to 26%), while increasing glutathione peroxidase expression. Unfortunately, due to the similar surface morphology of ferroptotic and apoptotic cells, SEM is not a reliable method for distinguishing between these two forms of cell death.
Conclusion: This study provides important insights into the mechanisms of toxicity of silica-coated SPIONs in endothelial cells and highlights the potential role of OA as a modulator of SPION-induced side effects.
Keywords: SPION, oleic acid, GPX4, ROS, ferroptosis, lipid peroxidation

Introduction

Ferroptosis, which was only conceptualized ten years ago, is an iron-mediated form of programmed cell death that was first proposed by Dixon in 2012.[1] It is driven by the accumulation of oxidized lipids in cellular membranes, due to the failure of cellular redox defiance mechanisms which prevent and repair membrane oxidative damage.

The key anti-ferroptotic mechanism in most cells depends on the activity of glutathione peroxidase 4 (GPX4) and its cofactor glutathione.[2] Key substrates for the lethal lipid peroxidation reaction are polyunsaturated fatty acyl (PUFA) chains esterified in membrane glycerophospholipids.[3] The initial products of lipid peroxidation are lipid hydroperoxides (LOOH), and the final products are reactive aldehydes, such as malondialdehyde (MDA) and 4-hydroxynonenal (4HNE), whose concentration increases during ferroptosis.[4] Ferroptosis cannot be prevented by chemical or genetic inhibitors effective in other types of regulated cell death, suggesting that this process is distinct from other mechanisms such as necrosis, autophagy, and apoptosis.[5]

15441

Increasing evidence has shown that ferroptosis is intimately associated with cancer initiation, progression, and suppression.[6] Previously, therapeutic strategies for cancer treatment have mainly focused on apoptosis. However, it has been found that apoptosis-based therapeutic strategies are not effective enough to achieve a satisfactory therapeutic effect in tumors because apoptosis is bypassed by the overexpression of apoptosis inhibitors and multi-drug resistance (MDR) of tumors. In addition, some cancers with RAS mutation exhibit intrinsic apoptosis resistance due to endogenous apoptosis inhibition associated with RAS mutation. Intriguingly, many different types of RAS-mutated cancer cells show sensitivity to the induction of ferroptosis.[7] Moreover, studies have shown that inducing ferroptosis can effectively reverse drug resistance, presenting a promising new avenue for cancer treatment.[6,8,9]

So far, numerous small molecule-based drugs have been reported to induce ferroptosis.[10] However, these compounds have significant drawbacks, including poor solubility, low therapeutic index, and off-target side effects. Various biomedical strategies have been explored to overcome these limitations, with ferroptosis-inducing nanoparticles (NPs) emerging as a particularly attractive alternative.[11] In fact, by synthesizing various iron-based nanomaterials that can passively target tumor sites and release exogenous iron in the lysosomes to increase the efficiency of the Fenton reaction,[12] cancer cells can be sufficiently and effectively killed via ROS accumulation. Additionally, the possibility to both load NPs with anti-cancer drugs (or ferroptosis inducers) and to surface-functionalize them to selectively target tumour cells, have been proven to enhance antitumor potency compared to ferroptosis-inducing small molecules.[11]

Among various iron-based NPs, superparamagnetic iron oxide nanoparticles (SPIONs) have been shown to be promising candidates for cancer therapy by various studies.[11] For example, the study by Huang et al[13] demonstrated that SPIONs induce oxidative stress and decrease autophagy activity in ovarian cancer stem cells, activate ferroptosis, and inhibit their proliferation, invasion, drug resistance, and tumorigenic ability. Zhang et al[14] demonstrated that SPIONs in human breast cancer cells (MCF7) induce the generation of ROS, which in turn induce cell death by ferroptosis by damaging mitochondria and cell membrane. The study by Zhentian et al[15] shows that Atranorin@SPIONs induce ferroptosis of gastric cancer stem cells by attenuating the expression of the Xc-/GPX4 axis and 5-hydroxymethylcytidine modification of mRNAs in this pathway, thereby achieving their therapeutic effect on gastric cancer. The study by Sang et al[16] provides a comprehensive ferroptosis treatment strategy using nanodevices with SPIONs to induce a lipid hydroperoxide burst and shorten the treatment time of epithelial cancer. Chen et al[17] constructed a novel microsphere co-loaded with Fe_3O_4 nanoparticles and adriamycin and showed that they could improve the treatment of advanced hepatocellular carcinoma by inducing ferroptotic cell death.

Although almost all NPs inducing ferroptosis have been tested in vivo and showed a favorable antitumor profile without significant side effects, no clinical trial with the reported NPs is currently ongoing, and information on their safety profile and effects on non-target tissues is lacking.[11] In fact, ferroptosis may also affect normal cells such as the vascular endothelium, possibly facilitating metastasis or causing undesired side-effects.[18] Tissue-specific *Gpx4* knockout study has shown that certain tissues and cells are much more susceptible to ferroptotic cell death than others, with the endothelium being one of the less sensitive tissues.[19] However, recent studies have shown that in endothelial cells ferroptosis strongly correlates with the development and progression of many vascular diseases, such as atherosclerosis,[20] diabetes-induced endothelial dysfunction,[21] diabetic retinopathy,[22] diabetic cardiomyopathy,[23] pulmonary hypertension,[24] and others,[25] suggesting that the interaction of SPIONs with endothelial cells could have several negative side effects for patients. Moreover, besides ferroptosis, SPIONs can also induce other forms of cell death depending on their size, surface coating, concentration, cell type, and experimental conditions.[26] The main types of cell death associated with SPIONs other than ferroptosis[13,27] include apoptosis,[28,29] necrosis,[30] autophagy,[28,31,32] and pyroptosis.[33] However, the characterization of cell death is often inconsistent across studies, with reductions in cell viability frequently being simplistically attributed to apoptosis.[34] For endothelial cells, understanding the type of cell death induced by SPIONs is particularly important for assessing their safety and clarifying their interactions with cellular systems. Interestingly, in our previous research[35] we showed that silica-coated SPIONs, upon internalization, can cause oxidative stress in HUVEC cells, leading to cell membrane damage and eventual cell death. Additionally, we found that exogenous oleic acid (OA) is protective against this SPION-induced damage, possibly because its incorporation into glycerophospholipids can cause the displacement of PUFA ultimately reducing the susceptibility of the cell membrane to lipid peroxidation.[36]

However, our previous work did not conclusively demonstrate that SPION-induced cytotoxicity in human umbilical vein endothelial cells (HUVEC) was mediated by ferroptosis. Thus, to address this key knowledge gap and better understand the potential, yet widely unexplored, side effects of SPION-based therapies on non-target endothelial cells we employed flow cytometry and Western blotting to assess particle effects on cell viability, ROS production, lipid peroxidation, and GPX4 expression. We also compared the effects on GPX4 and cell death with those induced by RSL3, a well-established ferroptosis inducer. In addition, we investigated the potential protective role of oleic acid (OA) as a modulator of SPION-induced ferroptosis and its relevance in mitigating off-target toxicity in endothelial cells. To achieve this goal, we compared the effects of OA with those of known ferroptosis inhibitors, such as α-tocopherol and ferrostatin-1. By elucidating these mechanisms, we aim to contribute to the development of nanomedicine strategies that are not only more effective but also safer for patients.

Finally, we used scanning electron microscopy to perform a comparative morphological study of cells undergoing ferroptosis, apoptosis, and SPION-induced cell death, aiming to highlight structural characteristics unique to ferroptosis that could serve as alternative markers to those conventionally detected using the gold standard method of transmission electron microscopy (TEM). By establishing reliable SEM-based markers, we aim to enable the identification of ferroptosis even in laboratories that lack access to TEM.

Materials and Methods
Materials
The chemicals used for the synthesis of maghemite (γ-Fe$_2$O$_3$) nanoparticles, and their silica coating were of reagent grade and purchased from commercial suppliers. Iron (III) sulfate hydrate, iron (II) sulfate heptahydrate (ACS, 99+%), tetraethyl orthosilicate (TEOS, 99.9%), and citric acid (99+%) were obtained from Alfa Aesar (Ward Hill, Massachusetts, USA). The acetone was purchased from AppliChem GmbH (Darmstadt, Germany); ethanol absolute from Carlo Erba (Cornaredo, Italy, reagent—USP); NH$_4$OH (aq) from Fluka (Gillingham, UK, p.a., 25%), and HCl 1 M p.a., from Riedl-de-Haën (Seelze, Germany). All these reagents were used as received. Deionized water was used for all aqueous preparations. Human umbilical vein endothelial cells (HUVEC) (ATCC) were kindly provided by Špela Zemljič Jokhadar (Institute of Biophysics, Faculty of Medicine, University of Ljubljana). Dulbecco's Modified Eagle Medium (DMEM) with high glucose content, foetal bovine serum (FBS), Hanks' balanced salt solution (HBSS), Dulbecco's phosphate buffered saline (DPBS), L-glutamine, fatty acid-free bovine serum albumin (FAF-BSA), α-tocopherol, staurosporine, 7-aminoactinomycin D (7-AAD), propidium iodide (PI), dithiothreitol (DTT), ethanol, tio-carbohydrase (TCH), osmium tetroxide (OsO$_4$), paraformaldehyde, NaH$_2$PO$_4$·2H2O, and Na$_2$HPO$_4$·2H$_2$O were purchased from Sigma Aldrich (St. Louis, USA); TrypLE Select was purchased from Life Technologies (Carlsbad, USA). Oleic acid (OA), RSL3, and ferrostatin-1 were purchased from Cayman Chemical (USA). BODIPY 581/591 C11, CM-H$_2$DCFDA, Annexin V-Pacific Blue Ready Flow Reagent, Tris-Glycine SDS Sample Buffer, Halt Phosphatase Inhibitor Cocktail, EDTA-Free Halt Protease Inhibitor Cocktail, Pierce 660 nm Protein Assay Kit, and Ionic Detergent Compatible Reagent were purchased from Thermo Fisher Scientific (Waltham, MA, USA). Nitrocellulose membrane was from Serva (Heidelberg, Germany), Western Blocking Reagent (WBR) and Lumi-Light Western Blotting Substrate Chemiluminescence Reaction Solution were purchased from Roche Applied Science (Penzberg, Germany), while horseradish peroxidase (HRP)-labelled secondary antibodies were from Jackson ImmunoResearch Laboratories (West Grove, PA, USA). Human GPX4 antibody (#52455) was from Cell Signaling Technology (Danvers, MA, USA), β-actin antibody (NB600-532) was from Novus Biologicals (Abingdon, UK), and glutaraldehyde and hexamethyldisiloxane (HMDS) were from SPI Supplies (West Chester, PA, USA).

Synthesis and Characterization of Silica-Coated SPIONs
Maghemite (γ-Fe$_2$O$_3$) nanoparticles were synthesized by co-precipitation from aqueous solutions of iron (II) and iron (III) salts, as previously described in our previous publications.[37–40] A solution of Fe^{2+} (0.027 mol L^{-1}) and Fe^{3+} (0.023 mol L^{-1}) was precipitated using 25% concentrated ammonia in two steps. First, the pH was raised to 3 and maintained for 30 minutes, leading to the precipitation of iron hydroxides. The pH was then increased to 11.6 to oxidize iron (II)

hydroxide, forming a spinel-structured maghemite. After aging for 30 minutes, the nanoparticles were thoroughly washed with deionized water, ethanol and acetone to remove impurities. Then, the surface of the iron oxide nanoparticles was decorated by grafting with citric acid and coated with a ~4 nm thick silica, as described in our published studies.[41–43] The obtained silica-coated SPIONs were characterized by transmission electron microscopy (TEM, JEOL 2100, Tokyo, Japan), Mössbauer spectroscopy, dynamic light scattering (DLS), polydispersity (PDI) calculation, and zeta potential measurements (Anton Paar GmbH, Litesizer 500, Graz, Austria) as described in detail in our published investigations.[35,44] Samples for TEM analysis were prepared by drying a drop of the aqueous suspension on a transparent carbon film on a copper grid. Due to the superparamagnetic properties of silica-coated maghemite nanoparticles they are here referred to as silica-coated superparamagnetic iron oxide nanoparticles (SPIONs).

Cell Culture Conditions and Treatments

HUVEC cells were cultured in complete culture medium (DMEM, 10% (v/v) FBS, 4 mM L-glutamine) in controlled atmosphere (37 °C, humidified conditions, 5% CO_2) and routinely split 2 times per week.

For experiments, cells were harvested with TrypLE Select and plated in complete culture medium at a seeding density of 3×10^4 cells/cm^2, then they were allowed to adhere for 24 hours before treatment. When co-exposure with OA (100 μM), α-tocopherol (1 mM), ferrostatin-1 (5 μM) or RSL3 (2 μM) was performed, these supplements were added 2 h before the exposure with silica-coated SPIONs (25 or 50 μg/mL) in serum-depleted medium and then the incubation lasted for additional 24 h. In the experiments where cells were treated exclusively with SPIONs, RSL3 or staurosporine (eg SEM imaging, phosphatidylserine exposure) the following concentrations were used: RSL3 (2 μM), staurosporine (0,3 μM) and SPIONs (25 or 50 μg/mL). 25 and 50 μg/mL SPIONs were used in assessing the ability of particles to induce lipid peroxidation, while 50 μg/mL SPIONs alone were used in the phosphatidylserine exposure assay and SEM / TEM imaging.

Notably, before addition to cell culture, OA was complexed with 0.02% fatty acid-free (FAF)-BSA, while α-tocopherol was complexed with 0.5% FAF-BSA in serum-depleted medium. In experiments with OA supplementation, control cells were grown in the presence of 0.02% FAF-BSA in serum-free medium. In experiments without OA supplementation, control cells were grown in serum-free medium.

The choice to use SPIONs at concentrations of 25 and 50 μg/mL was based on cytotoxicity data from our previous study (Repar et al, 2022).[35] In that work, we found that treatment with 5 and 10 μg/mL of silica-coated SPIONs caused only mild cytotoxic effects in HUVEC after 24 hours. Therefore, concentrations equal to or below 25 μg/mL may not produce a suitable response to reliably study the protective role of oleic acid.

Lipid Peroxidation Assay with BODIPY 581/591 C11

Cellular lipid ROS levels were measured by flow cytometry using the oxidation sensitive BODIPY 581/591 C11 dye (BODIPY 581/591 undecanoic acid). HUVEC cells were seeded at a density of 3×10^4 cells/cm^2 in 24-well plates. They were grown in 500 μL of complete medium. After 24 hours, cells were washed with PBS and stained with 300 μL of 1 μM BODIPY 581/591 C11 dye in HBSS for 30 minutes at 37°C. Cells were washed to remove the remaining dye and exposed to chemicals and SPIONs. After 24 hours, cells were detached using TrypLE Select, transferred to tubes for flow cytometry, centrifuged, and the cell pellet resuspended in 300 μL HBSS. Cells were placed on ice and analysed using a FACSMelody cell sorter (Becton Dickinson, Franklin Lakes, NJ, USA). The oxidised form of the BODIPY 581/591 dye was excited with a 488-nm laser, and the signal was detected with the 527/32 filter. The reduced form of the dye BODIPY 581/591 was excited with a 561-nm laser, and the signal was acquired with the 697/58 filter. The analysis was performed with a minimum of 20,000 events per sample. The degree of lipid peroxidation was calculated as the ratio of the geometric mean (GM) of the fluorescence intensities of the oxidised dye and the reduced dye. Cells were gated as shown in Supplementary Figure 1.

ROS and Cell Death Detection Using CM-H$_2$DCFDA and 7-AAD

Reactive oxygen species (ROS) and cell death were determined by flow cytometry as described previously.[45] Cells with damaged membranes stain with 7-AAD, while living cells with intact cell membranes remain dark. HUVEC cells were

seeded in 24-well plates and treated as described in the "Cell Culture Conditions and Treatments" section. 24 hours after treatment, cells were stained with 1 μM CM-H$_2$DCFDA in HBSS for 30 minutes at 37°C followed by a 2 h recovery period in DMEM phenol red-free medium. Then, cells were detached and collected in tubes for flow cytometry and 7-AAD was added at a final concentration of 5 μM. Cells were incubated at room temperature for 10 minutes, centrifuged and the cell pellet resuspended in 300 μL HBSS. Cells were placed on ice and analysed using a FACSMelody cell sorter (Becton Dickinson, Franklin Lakes, NJ, USA). The 7-AAD was excited with a 488-nm laser, and the signal was detected with the 700/54 filter. The CM-H$_2$DCFDA was excited with a 488-nm laser, and the signal was acquired with the 527/32 filter. The analysis was performed with a minimum of 20,000 events per sample. The gating strategy used in these experiments is identical to that applied in the BODIPY assay, with the only difference being that ROS production was quantified exclusively in 7-AAD-negative (viable) cells.

Phosphatidylserine Exposure Assay

The phosphatidylserine (PS) exposure was determined by flow cytometry using Annexin V-Pacific Blue and PI. Annexin V labels PS on the extracellular membrane. PI binds to double-stranded DNA but is excluded from cells with intact plasma membranes, which makes it a standard reagent used to assess cell viability. HUVEC cells were seeded in 24-well plates and treated as described in the "Cell Culture Conditions and Treatments" section. 24 hours after treatment, floating and adherent cells were collected and stained with 3 μL Annexin V-Pacific Blue Ready Flow and PI with final concentration of 1.7 μg/mL at room temperature for 10 minutes. Cells were placed on ice and analysed using a FACSMelody cell sorter (Becton Dickinson, Franklin Lakes, NJ, USA). Pacific Blue was excited with a 405-nm laser, and the signal was detected with the 528/45 filter. PI was excited with a 561-nm laser, and the signal was acquired with the 613/18 filter. The analysis was performed with a minimum of 20,000 events per sample.

Western Blot Analysis of Cellular GPX4 Protein Content

The protein level of GPX4 was determined by Western blot analysis, a common method for the detection and analysis of proteins. HUVEC cells were seeded in 6-well plates and treated as described in the "Cell Culture Conditions and Treatments" section. Cell lysates were prepared by scraping cells into lysis buffer (composition: Tris-glycine SDS sample buffer, 800 mM DTT, phosphatase inhibitors, and protease inhibitors). Cell lysates were denatured at 95°C for 10 minutes and stored on ice. Protein concentration of the samples was measured using the Pierce 660-nm protein assay kit with the addition of ionic detergent-compatible reagent. 10 μg of total protein were separated by SDS-PAGE on 10% poly-acrylamide gels and transferred to a nitrocellulose membrane. After the transfer, the membrane was blocked for 1 hour at room temperature by gentle shaking in 5% non-fat dry milk in TBS buffer (50 mM Tris-HCl, pH 7.5; 150 mM NaCl) for the detection of GPX4 and in 1% Western blocking reagent (WBR) in the TBS buffer for detection of β-actin. Primary rabbit monoclonal antibodies to human GPX4 were diluted 1:1000 in 5% non-fat dry milk in TBS/0.1% Tween-20 (TBST) buffer, and primary antibodies to β-actin (#NB600-532, Novus Biologicals, Abingdon, UK) were diluted 1:5000 in 0.5% WBR in TBS buffer. Membranes were incubated with the primary antibodies overnight at 4°C with gentle shaking. After washing with TBST, the membranes were incubated for one hour at room temperature with gentle shaking with horseradish peroxidase-conjugated secondary antibody solution diluted 1:10000 in 0.5% WBR in TBS buffer. After washing with TBST buffer, the membrane was incubated in Lumi-Light Western Blotting Substrate Chemiluminescence Reaction Solution for 1 minute and then photographed using a ChemiDoc XRS+ (Biorad, Hercules, CA, USA). The intensity of the bands on the blots was quantified using ImageJ (National Institutes of Health, Washington, DC, USA) and normalized to the loading control β-actin.

Scanning Electron Microscopy

Scanning electron microscopy (SEM) is a type of electron microscope that produces images of a sample by scanning its surface with a focused electron beam, enabling high-resolution imaging. This SEM an ideal technique for studying cell shape and surface morphology that cannot be clearly visualized with a light microscope. HUVEC cells were seeded in 12-well plates prepared with coverslips and treated as described in the "Cell Culture Conditions and Treatments" section. Coverslips containing adherent cells were washed in DPBS for 30 minutes. Cells were then fixed for 48 hours at 4°C in

Karnovsky fixative prepared from 2.5% glutaraldehyde and 0.4% paraformaldehyde in 1 M NaH_2PO_4-$2H_2O$ and Na_2HPO_4. Cells were washed with 1 M DPBS, fixed with 1% OsO_4, and rinsed with distilled water. Cell surfaces were washed in supersaturated and filtered TCH solution, rinsed with distilled water, fixed with 1% OsO_4, and rinsed again with distilled water. Samples were dehydrated with ethanol at concentrations of 30%, 50%, 70%, 80%, 90% and absolute ethanol. Further dehydration steps were performed with a mixture of HMDS and absolute ethanol at ratios of 1:2 and 1:1, and with absolute HMDS. After 24 hours, the samples were coated with a 6 nm thick Au/Pd layer using a precision etching and coating system (PECS Gatan 682, Pleasanton, CA, USA). Scanning electron microscopy was performed using a JEOL JSM-6500F scanning electron microscope (JEOL, Tokyo, Japan).

Transmission Electron Microscopy

HUVEC cells were seeded at a density of 3×10^4 cells/cm^2 on Falcon™ Cell Culture Inserts (Thermo Fisher Scientific Inc., Waltham, MA, USA) in culture medium and grown in a controlled atmosphere for one day. Cells were then left untreated or incubated with 50 µg/mL of silica-coated SPIONs for 24 h in serum-free medium. Afterwards, cells were washed three times with PBS and then fixed with a mixture of 4% (w/v) formaldehyde and 2% (w/v) glutaraldehyde in 0.1 M cacodylate buffer (pH 7.4) for 3 h at 4°C. Overnight rinsing in 0.33 M sucrose in 0.2 M cacodylate buffer was followed by the post-fixation in 1% osmium tetroxide in 0.1 M cacodylate buffer for 1 h. After the dehydration in graded ethanol, the samples were embedded in Epon 812 resin (Electron Microscopy Sciences, Hatfield, PA, USA), and ultrathin sections were cut with an ultramicrotome Leica EM UC6. A Philips CM100 TEM (Eindhoven, The Netherlands) operated at 80 kV was used to image the samples.

Statistical Analysis

Statistical analysis was performed using GraphPad Prism Software Version 6.01. Data are presented as means ± SEM. Statistical significance was determined using one-way ANOVA or two-way ANOVA, followed by Tukey's or Dunnett's post-hoc test. P-values < 0.05 were considered statistically significant (*p < 0.05, **p < 0.01, ***p < 0.001, ****p < 0.0001).

Results

Characteristics of Silica-Coated SPIONs

After synthesis, silica-coated superparamagnetic iron oxide nanoparticles (SPIONs) were characterized using various methods. The zeta potential value in serum-free cell culture medium was found to be −18.7 ± 1.6 mV (Figure 1A), and dynamic light scattering (DLS) measurements revealed a mean hydrodynamic diameter of 57 nm and a polydispersity index (PDI) of 0.23 (Figure 1B).[35] The mean size of the particles, as determined by analysis of transmission electron microscopy (TEM) images (N > 100), was approximately 11 nm (Figure 1C), while the thickness of the silica shell after coating was about 4 nm (Figure 1D), resulting in a final diameter of 19.3 ± 2.0 nm. As reported in our previous works, the X-ray diffraction (XRD) of the precipitated iron oxides showed a single spinel phase, whereas the Mössbauer spectroscopy confirmed that the SPIONs were composed of maghemite (γ-Fe_2O_3).[35,44]

Silica-Coated SPIONs Induce Lipid Peroxidation

In our previous study, we showed that silica-coated SPIONs induced cell death in endothelial cells, as determined by resazurin, neutral red uptake, and CyQUANT assays, and that such cytotoxic effects were associated with oxidative stress and cell membrane alterations.[35] However, in that study, we did not conclusively demonstrate that SPION-induced cytotoxicity in human umbilical vein endothelial cells (HUVEC) was mediated by ferroptosis.

Thus, in the present work, we first investigated whether silica-coated SPIONs could induce lipid peroxidation, a hallmark of ferroptosis, in endothelial cells. For this purpose, we stained the cells with the lipid ROS sensor BODIPY 581/591 C11 (BODIPY) and exposed them to different concentrations of silica-coated SPIONs for 24 hours. Fluorescence data were then collected via flow cytometry using the gating strategy described in Supplementary Figure 1. The obtained results showed that particles increased lipid peroxidation in human umbilical vein endothelial cells (HUVEC) in a concentration-dependent manner (Figure 2A and B).
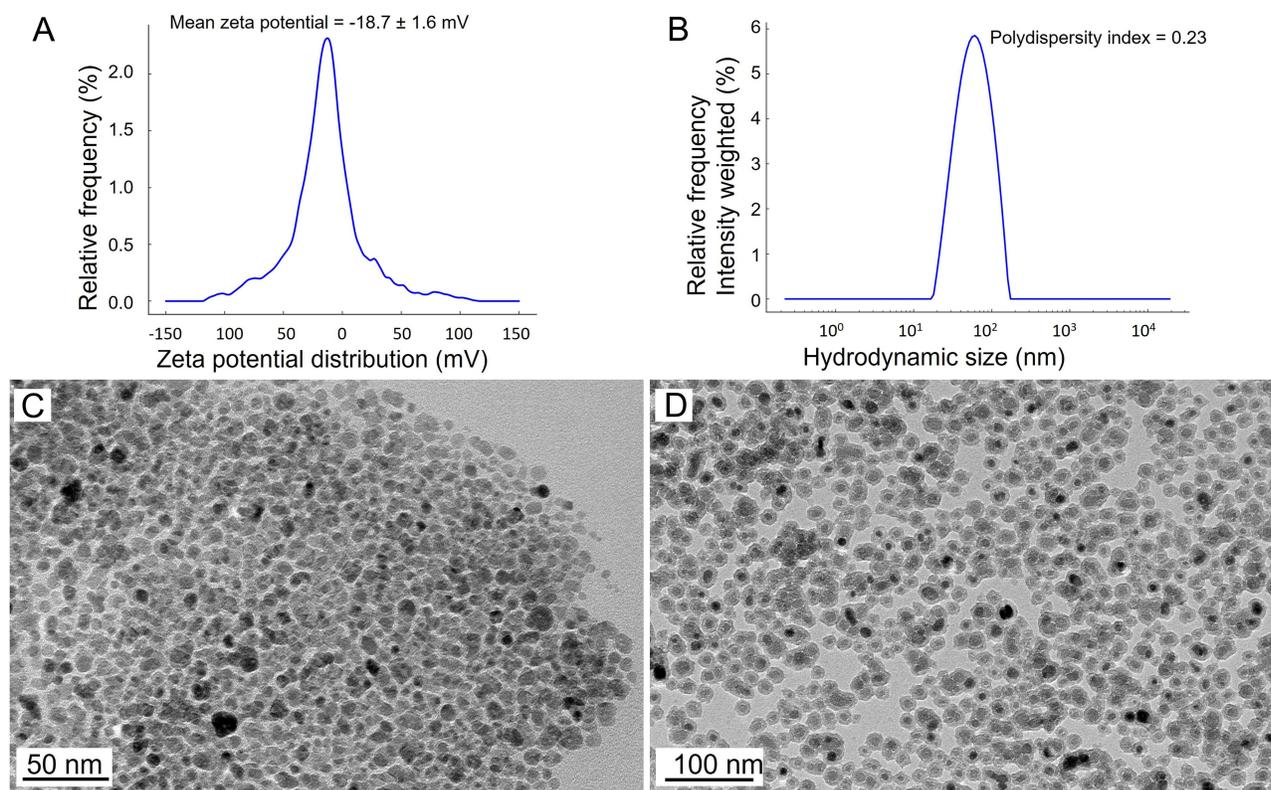
Figure 1 Nanoparticle characterization. Zeta potential distribution of silica-coated superparamagnetic iron oxide nanoparticles (SPIONs) in serum-free medium (**A**), hydrodynamic size distribution and polydispersity index of silica-coated SPIONs in serum-free medium (**B**), and representative transmission electron microscopy (TEM) images of as-synthesized SPIONs (**C**), and silica-coated SPIONs (**D**).
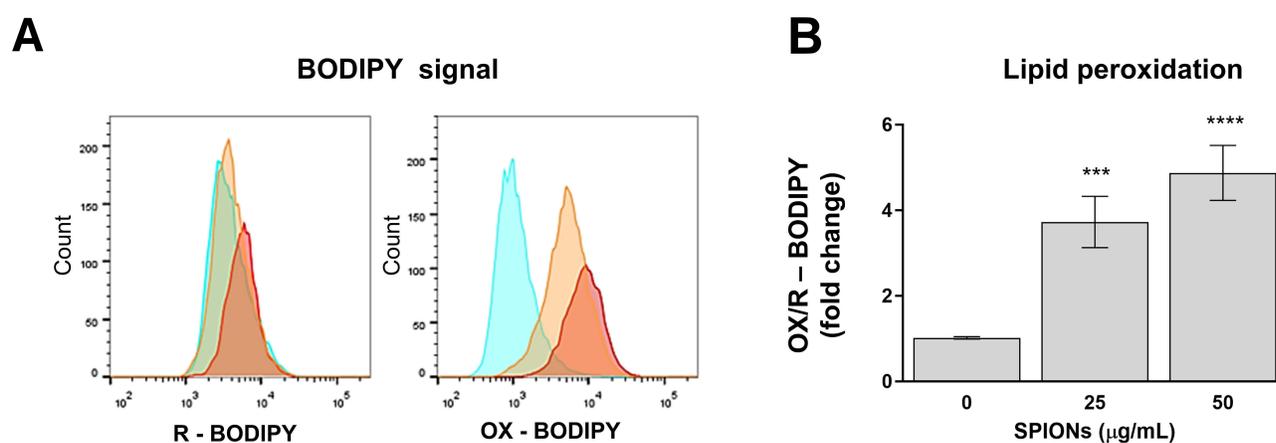

Figure 2 Silica-coated SPIONs increased lipid peroxidation in HUVEC cells in a concentration-dependent manner. Human umbilical vein endothelial cells (HUVEC) were stained with BODIPY 581/591 C11 dye (BODIPY), a lipid peroxidation indicator, and exposed to various concentrations of silica-coated superparamagnetic iron oxide nanoparticles (SPIONs) for 24 hours and then analysed by flow cytometry. The data are presented as follows: (**A**) Representative flow cytometry histograms showing the fluorescence emission of oxidized (OX) and reduced (R) BODIPY in untreated control cells (light blue) and in cells treated with 25 μg/mL (orange) or 50 μg/mL (red) SPIONs. (**B**) Quantification of lipid peroxidation, expressed as fold change of the OX/R BODIPY geometric mean fluorescence intensity (MFI) ratio in SPION-treated cells versus the same ratio calculated in untreated control cells (± SEM). Data represent the mean of at least three independent experiments. Statistical significance is indicated as: ***$P < 0.001$; ****$P < 0.0001$.

15447

Ferroptosis Inhibitors and Oleic Acid Decrease Lipid Peroxidation, Oxidative Stress, and Cell Death Caused by Silica-Coated SPIONs

Since excessive lipid peroxidation plays a central role in the process of ferroptotic cell death, we next tried to confirm if ferroptosis was involved in the cytotoxic effects triggered by silica-coated SPIONs.

To do so, we first tested whether α-tocopherol and ferrostatin-1, lipophilic antioxidants and potent inhibitors of ferroptosis, could reduce the SPION-induced rise in cell death, oxidative stress, and lipid peroxidation (Figure 3A–C). Then, we also investigated the effect of OA, which has previously been shown to inhibit ferroptosis in nanoparticle-free experiments, by displacing oxidizable PUFAs from membrane phospholipids,[36] and to protect endothelial cells from SPION-induced toxicity.[35]

As presented in Figure 3, in cells exposed to a lower concentration (25 μg/mL) of silica-coated SPIONs, ferrostatin-1 and α-tocopherol fully suppressed the SPION-induced lipid peroxidation and partially reduced ROS formation, however, no significant effects on cell death were detected. Similarly, OA supplementation significantly mitigated the SPION-elicited rise
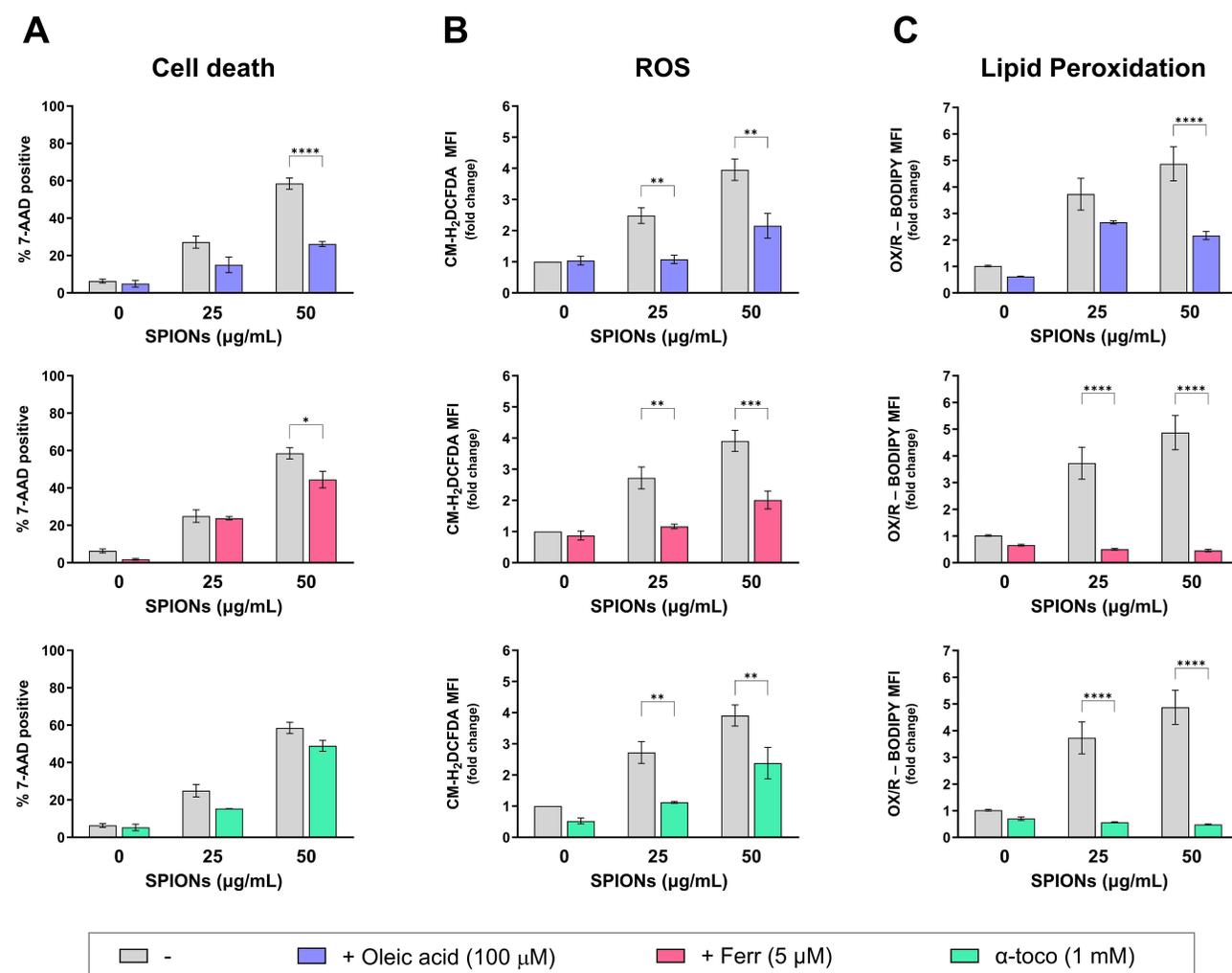

Figure 3 Ferroptosis inhibitors decrease lipid peroxidation, oxidative stress, and cell death caused by silica-coated SPIONs. To quantify ROS production and cell death (**A** and **B**), HUVEC were exposed to SPIONs and/or selected ferroptosis inhibitors or oleic acid for 24 hours and then stained with CM-H$_2$DCFDA and 7-AAD dyes and analysed via flow cytometry. Data are presented either as % of 7-AAD positive cells or as fold change of the CM-H$_2$DCFDA MFI signal calculated versus the MFI of control cells. To measure lipid peroxidation instead (**C**), cells were first stained with the lipid peroxidation sensor, BODIPY, and then exposed to silica-coated SPIONs and/or selected ferroptosis inhibitors or oleic acid for 24 hours and subsequently analysed via flow cytometry. The data in the graphs show the ratio of the MFI of the oxidized (OX) and reduced (R) BODIPY dye of a specific sample normalized by the same ratio calculated in untreated control cells. Bars show mean values (± SEM) calculated from at least three independent experiments. Only statistical significance within the same sample ± ferroptosis inhibitors or oleic acid is shown (*$P < 0.05$; **$P < 0.01$; ***$P < 0.001$; ****$P < 0.0001$).

Abbreviations: HUVEC, human umbilical vein endothelial cells; SPIONs, superparamagnetic iron oxide nanoparticles; MFI, geometric mean fluorescence intensity; BODIPY, BODIPY 581/591 C11; ROS, reactive oxygen species; CM-H$_2$DCFDA, 5-(and-6)-chloromethyl-2′,7′-dichlorodihydrofluorescein diacetate; 7-AAD, 7-Amino-actinomycin D.

in ROS levels and reduced cell death but was less potent in the prevention of lipid peroxidation when compared to the other ferroptosis inhibitors. In cells exposed to a higher concentration (50 µg/mL) of silica-coated SPIONs, although the ferroptosis inhibitors reduced lipid peroxidation to the level measured in unexposed cells, they could not fully block the rise in oxidative stress and cell death caused by the treatment. OA instead, significantly reduced all tested parameters with a more potent effect in the reduction of cell death. In Supplementary Figure 2 are shown some representative flow cytometry histograms showing the effects of α-tocopherol, OA and ferrostatin-1 on lipid peroxidation and ROS production in 50 µg/mL-treated cells.

The protective role of OA was further confirmed using several complementary approaches, as shown in Supplementary Figure 3A–C. OA significantly reduced SPION-induced cell death, as measured by the resazurin assay. It also lowered particle-induced lipid peroxidation, as demonstrated by time-course flow cytometry and fluorescence microscopy. RSL3, a known ferroptosis inducer, was included as a positive control in these experiments.

Silica-Coated SPIONs Induce Ferroptosis via Decreasing GPX4 Expression

GPX4 plays a central role in counteracting ferroptosis, mainly through the reduction of lipid hydroperoxides to their corresponding alcohols. Moreover, down-regulation of GPX4 is frequently studied as a biomarker for the detection of ferroptotic cell death.[27] Therefore, we next examined how silica-coated SPIONs affect GPX4 protein content in HUVEC cells. We also examined the effect of α-tocopherol, ferrostatin-1, and OA. The covalent GPX4 inhibitor RSL3, was used as a positive control.

Our results showed that RSL3, silica-coated SPIONs, and a combination of both, downregulated GPX4 expression compared with unexposed cells. It is also evident that α-tocopherol, ferrostatin-1, and OA increased GPX4 expression in cells exposed to SPIONs, and this increase was statistically significant in the case of ferrostatin-1 (Figure 4A and B).

Silica-Coated SPIONs Do Not Induce Phosphatidylserine Externalization

Phosphatidylserine (PS) is usually found on the inner leaflet of the plasma membrane and its exposure on the cell surface is a marker of apoptosis. We investigated PS exposure in HUVEC cells undergoing apoptosis, ferroptosis, and cell death induced by 50 µg/mL of silica-coated SPIONs. Using Annexin V-Pacific Blue to bind exposed PS, and propidium iodide (PI) to stain dead cells (necrotic cells and post-apoptosis necrotic cells),[46] we identified different cell populations: viable
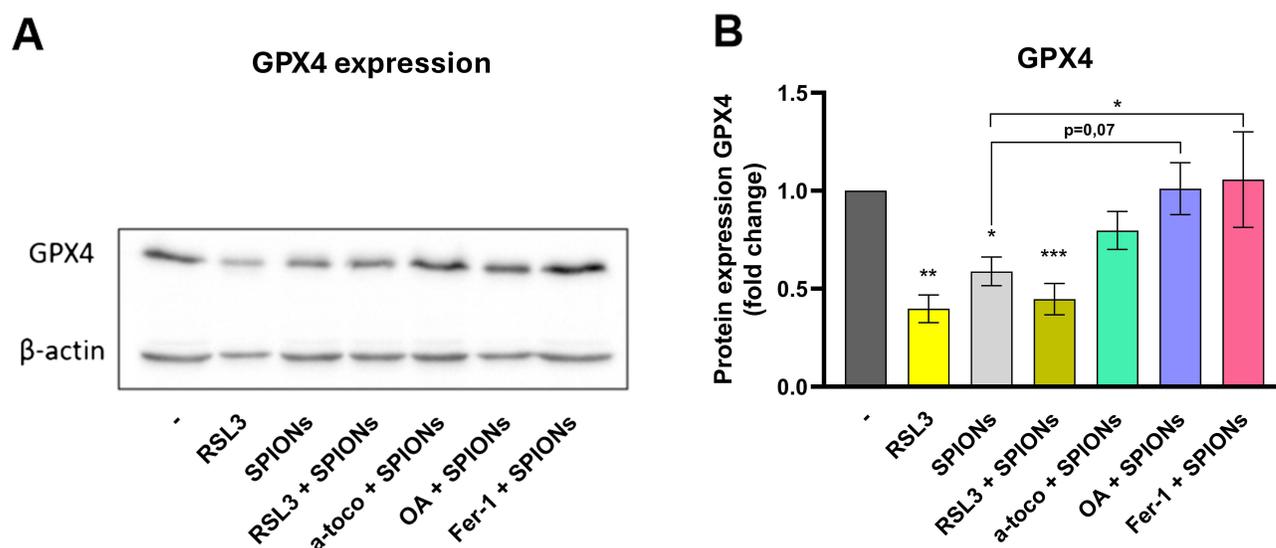

Figure 4 Silica-coated SPIONs induce ferroptosis via decreasing GPX4 expression. HUVEC were seeded in 6-well plates and exposed to oleic acid, selected ferroptosis inductors or inhibitors and/or silica-coated SPIONs (50 µg/mL) for 24 hours. After 24 hours, cells were lysed, proteins in the cell lysates were separated by polyacrylamide gel electrophoresis in the presence of SDS, and Western blotting was performed, followed by immunodetection of GPX4 and β-actin proteins on a nitrocellulose membrane (**A**). The spots on the membrane were analysed densitometrically using ImageJ. Data in the graph shows the ratio of GPX4 to β-actin protein band intensities normalized to their corresponding values in unexposed cells. In (**B**) are shown the mean values of four biological replicates of the experiment (± SEM). Values that are statistically significantly different from controls or a specified sample are indicated (*P < 0.05; **P < 0.01; ***P < 0.001; ****P < 0.0001).

Abbreviations: a-toco, α-tocopherol; Fer-1, ferrostatin-1; -, untreated control cells; OA, oleic acid; GPX4, glutathione peroxidase 4; human umbilical vein endothelial cells, HUVEC; superparamagnetic iron oxide nanoparticles, SPIONs; RSL3, RAS-selective lethal 3.
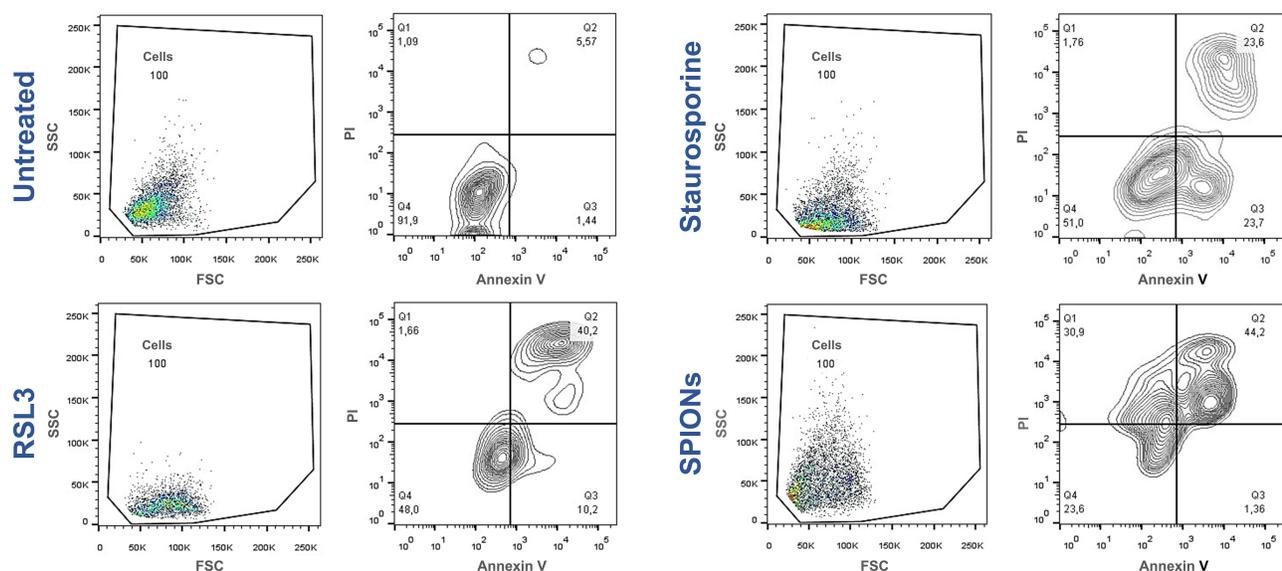
Figure 5 Silica-coated SPIONs do not induce PS exposure. Cells were exposed to ferroptosis inducer RSL3, apoptosis inducer staurosporine and silica-coated SPIONs for 24 hours and then double stained with Annexin V-Pacific blue and PI. The cells were then analysed using a flow cytometer. The dot plots (left) show the cell population identified by FCS and SSC selected for further analysis of PS exposure and cell viability, which is shown in the contour plots (right). The lower left quadrant represents double-negative cells that are viable and do not have exposed PS, the lower right quadrant represents Annexin V-positive and PI-negative cells with intact cell membrane and exposed PS, and the upper right quadrant represents double-positive cells that have lost cell membrane integrity.
Abbreviations: PI, propidium iodide; PS, phosphatidylserine; FCS, forward scatter; SSC, side scatter; SPIONs, super paramagnetic iron oxide nanoparticles; RSL3, RAS-selective lethal 3.

cells (double negative), cells with exposed PS (Annexin V-positive, PI-negative) which are apoptotic, and dead cells (double positive) (Figure 5).

Untreated cells were mostly double negative. Staurosporine-treated cells showed three populations: viable, PS-exposed, and dying cells. RSL3-treated cells had fewer PS-exposed cells but more dead/necrotic cells. Silica-coated SPION-treated cells had almost no Annexin V-positive PI-negative cells, suggesting their cell death mechanism aligns more with ferroptosis than apoptosis.[35]

Silica-Coated SPIONs Induce Morphological Changes of Cells Observed by SEM, Which are Confirmed as Ferroptotic by TEM

The scanning electron microscopy (SEM) examination provides information about cell-cell and cell-substrate interactions, cell surface changes, including membrane blebbing and loss of features such as microvilli.[46,47] Here we used the SEM images to assess changes in cell shape, as well as in the presence of extracellular vesicles and protrusions, following treatments with SPIONs, RSL3 and staurosporine (Figure 6).

Cell Shape

In the untreated cells, we mainly observed attached polygonal cells with diameters of up to 60 μm, which in some cases are completely attached to the substrate, in others only partially. In addition to the flat cells, spherical cells with diameters of up to 20 μm are also observed detaching from the substrate, indicating that they are dying cells. In cells exposed to staurosporine, RSL3 and silica-coated SPIONs, we observe a lower density of flat cells and a higher density of spherical dying cells. These data matched the results obtained with flow cytometry where RSL3 cells and SPIONs had a higher number of double-positive cells.

Extracellular Vesicles and Cell Blebbing

In cells treated with staurosporine, we observe extracellular vesicles as well as spheroidal cells with blebs up to 5 μm in diameter on the cell surface, which corresponds to the phenomenon of "cell blebbing" that has been associated with various physiological and pathological processes (apoptosis, necrosis, ferroptosis).[48] In cells treated with RSL3 and SPIONs, extracellular vesicles and the phenomenon of cell blebbing are also present. In contrast, in untreated cells, extracellular vesicles are very rare and no cell blebbing is observed.
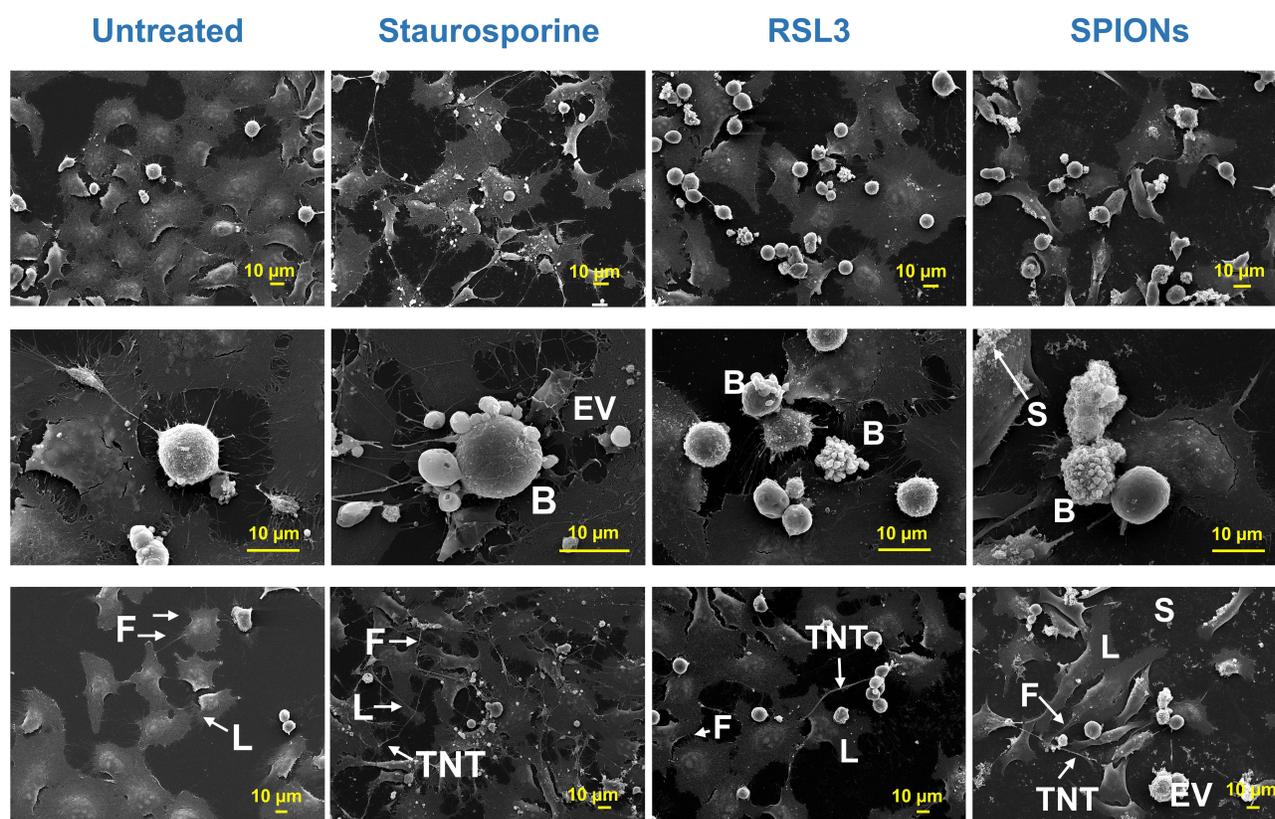
Figure 6 SEM micrographs of cells exposed to staurosporine, RSL3, and SPIONs.
Abbreviations: EV, extracellular vesicle; B, cell blebbing; F, filopodia; L, lamellipodia; TNT, tunnelling nanotube; S, silica-coated super paramagnetic iron oxide nanoparticles (SPIONs); RSL3, RAS-selective lethal 3.

Cell Protrusions

Lamellipodia and filopodia are cell protrusions that appear on the leading edges of migrating cells and function in sensing the cell environment and in making initial, dynamic adhesions to extracellular matrix and other cells.[49] In untreated cells, numerous uniform flat complexes are observed at the cell edges, through which cells closer to each other form a flat junction with a diameter of more than 10 μm. The observed structures are likely to be lamellipodia, actin structures at the cell edges that attached cells use for mobility and the formation of cell junctions.[50,51] In addition, a series of 1–15 μm long protrusions is clearly visible at the cell edges that contact the substrate and, in some cases, form contacts with neighbouring cells. We hypothesize that these are filopodia, thin (0.1–0.2 μm), finger-like outgrowths that are also part of the actin network.[52,53] Under stress conditions induced by treatment with staurosporine, RSL3, and SPIONs, cells exhibited the formation of both lamellipodia and filopodia, along with a marked increase in thin, elongated protrusions that may resemble tunneling nanotubes (TNTs).[54–56] However additional experiments are needed to confirm this hypothesis.

In addition to lamellipodia and filopodia, staurosporine also induced the expansion of a very large number of unbranched, actin-based long cell extensions that reached up to 30 μm and extended not only from the free cell edge but also from the cell-cell junctions.

Overall, we were unable to distinguish between cells dying by ferroptosis and those dying by apoptosis using SEM. Thus, TEM was performed in untreated and SPION-treated cells to confirm ferroptosis.

Ultrastructural Hallmarks of Ferroptosis in TEM

TEM of untreated samples (Figure 7A–C) showed healthy, flat cells firmly attached to the surface (Figure 7A). The mitochondria (stars) displayed numerous cristae and a uniform matrix, suggesting normal function. Several Golgi apparatus (G) and multivesicular bodies (MB) were also observed. Centrioles (C) are clearly visible in Figure 7B.
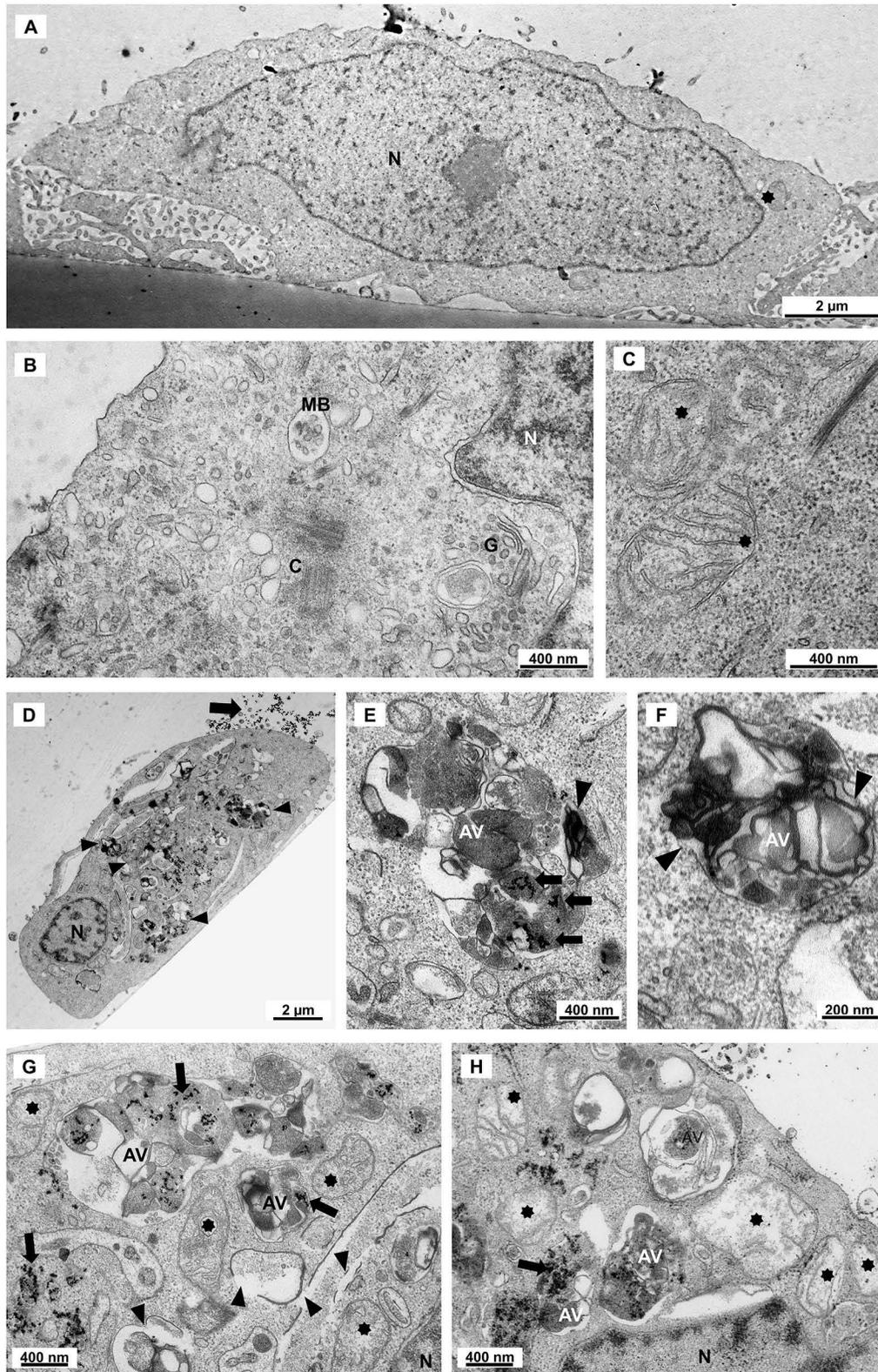
Figure 7 TEM micrographs of untreated cells and cells exposed to SPIONs. (**A–C**) images of untreated cells. (**D–H**) images at different magnifications of cells undergoing ferroptosis in response to the treatment with 50 µg/mL SPIONs.

Abbreviations: N, nucleus; MB, multivesicular body; G, Golgi apparatus; C, centrioles; AV, autophagic vacuoles; stars, mitochondria; arrow, silica-coated super paramagnetic iron oxide nanoparticles (SPIONs); arrowhead, fragmented inner membranes.

Cells treated with SPIONs instead (Figure 7D–H), revealed many roundish cells with plasma membrane blebbing, vesiculation, and even rupturing, indicating that they were dying cells (eg Figure 7D and H). The most prominent ultrastructural change of these cells was swollen mitochondria (stars) with electron-lucent matrix and a highly reduced number of cristae as a typical sign of ferroptosis (Figure 7G and H). Besides drastically altered mitochondria, we also found in the cytosol of these cells some fragmented inner membranes (arrowheads), numerous autophagic vacuoles (AV) with internalized SPIONs (arrows), various organelles in different stages of degradation, and even membranes. Some of the membranes in the autophagic vacuoles were thick and highly electron-dense and resembled myelin membranes (Figure 7G). In addition, we also detected dilated ER cisternae and disintegration of the Golgi apparatus.

Discussion

In this study, we demonstrate that exposure to silica-coated superparamagnetic iron oxide nanoparticles (SPIONs) in endothelial cells leads to increased lipid peroxidation (LP) and reactive oxygen species (ROS) production, along with a reduction in GPX4 expression which collectively induces ferroptotic cell death. Unfortunately, unlike transmission electron microscopy (TEM), scanning electron microscopy (SEM) images revealed no ferroptosis-specific morphological features when these samples were compared to cells undergoing staurosporine-induced apoptosis. Furthermore, we show here that treatment with oleic acid (OA, 100 μM), similarly to ferrostatin-1 and α-tocopherol, attenuates SPION-induced oxidative stress and lipid peroxidation, potentially by mitigating GPX4 downregulation. Notably, OA proved to be the most effective treatment at preventing ferroptotic cell death, despite being the least effective among the three compounds at suppressing lipid peroxidation.

Silica-Coated SPIONs Induce Ferroptosis

Ferroptosis, a regulated cell death characterized by lipid peroxidation, has been difficult to identify due to the lack of a specific marker.[57] Our previous research suggested the potential involvement of ferroptosis in endothelial cells exposed to silica-coated SPIONs, based on oxidative stress and changes in membrane composition. In this study, we confirmed ferroptosis induction by measuring lipid peroxides and GPX4 levels, a key enzyme involved in preventing lipid peroxidation and subsequent ferroptosis.[58]

To further validate ferroptosis, we employed two fat-soluble ferroptosis inhibitors, α-tocopherol and ferrostatin-1, which scavenge lipid radicals.[59] We hypothesized that if these inhibitors reduced lipid peroxidation and restored GPX4 levels, this would support the occurrence of ferroptosis in our model. We confirmed that both ferroptosis inhibitors reduced lipid peroxidation and ROS production in cells treated with 50 and 25 μg/mL SPIONs, indicating that ferroptosis contributes to particle-induced cytotoxicity. Notably, the inhibitors were more effective at reducing lipid peroxidation than overall ROS levels which may be due to their lipophilic nature, which allows them to embed in cellular membranes and act directly at the sites where lipid peroxides are generated. In contrast, since ROS are produced across various cellular compartments, they are more challenging to neutralize effectively.

However, ferroptosis inhibitors did not fully suppress cell death in contrast to OA which not only reduced cell death from 58% to 26% in 50 μg/mL SPION-treated samples but also reduced lipid peroxidation and ROS formation in endothelial cells. Such effect might be linked to the mechanism of action of OA, which, once incorporated into the membrane phospholipids in place of polyunsaturated fatty acids (PUFAs), has been proven to be less susceptible to lipid peroxidation than its polyunsaturated counterparts,[35,36,60] possibly helping to prevent particle-induced membrane rupture and cell death. Notably, the mild lipid peroxidation observed in OA- and SPION-co-treated cells may be influenced by the detection method used. BODIPY 581/591 C11 is a fat-soluble, oxidation-sensitive dye that responds to oxidative stress by shifting its fluorescence emission, thereby indicating the intensity of lipid peroxidation reactions within the cells. However, it does not directly quantify the absolute amount of lipid peroxides present in cell membranes at a given time. As a result, membranes enriched with oleic acid, which are more resistant to oxidation, may still appear positive when stained with BODIPY, since the dye itself can be still oxidized by intracellular reactive oxygen species (ROS), regardless of the actual susceptibility of the membrane lipids. It is important to note that while OA provides higher resistance to oxidation in comparison to PUFAs, it does not work directly as an antioxidant in the same way as α-tocopherol or ferrostatin-1, which actively inhibit lipid peroxidation acting as radical scavengers.

In contrast, the stronger ability of OA to prevent cell death compared to ferroptosis inhibitors is quite puzzling. Unlike α-tocopherol and ferrostatin-1, OA is a fatty acid and can possibly serve as an energy source for the cell, providing a metabolic advantage to cells exposed to stress conditions like SPION-induced ferroptosis. Another hypothesis could be linked to the nature of the stressor used in these experiments, the silica-coated SPIONs. In fact, it is known that nanomaterial-induced toxicity is not limited to the production of ROS and lipid peroxides; other mechanisms such as lysosomal permeabilization or hyperpolarization have also been reported, the latter being demonstrated for silica nanoparticles.[61,62] Interestingly, Rachid Skouta and colleagues showed that ferrostatin-1 protects against lipid peroxidation but not against ROS formation or lysosomal permeabilization in disease models.[63] Although ferrostatin-1 has been shown to still reduce cell death in these experiments, those studies did not involve nanomaterials, which can potentially significantly alter cell death dynamics. Silica-coated SPIONs, for example, are known to persist in human cells for prolonged periods, where they may exert also a mechanical stress on different organelles (eg lysosomes and endosomes), potentially triggering alternative forms of cell death once ferroptosis is inhibited. Monounsaturated fatty acids (MUFAs), such as oleic acid, have also been associated with lysosomal permeabilization and cell death, similar to nanoparticles.[64] However, in our earlier work,[35] we showed that 100 μM of oleic acid (an amount consistent with high dietary intake), was non-toxic to HUVECs and could be safely applied before SPION exposure. Therefore, it remains possible that low concentrations of oleic acid, differently from ferrostatin-1, may protect against SPION-induced cell death, acting on membrane structure, composition and physical properties. However, further experiments are needed to explore this possibility.

When measuring the expression of GPX4, we used RSL3, a well-established selective ferroptosis inducer, as a positive control. RSL3 is known to inhibit GPX4 activity, a key enzyme in preventing ferroptotic cell death.[65] Previous research has demonstrated that induction of ferroptotic cell death with RSL3 often results in the reduction of GPX4 protein levels.[65] In accordance, we observed a significant decrease in GPX4 cellular content after treatment with RSL3. Importantly, silica-coated SPIONs also led to a decrease in GPX4 levels, suggesting that SPIONs compromise endothelial cell viability through a mechanism that includes GPX4 reduction leading to insufficient removal of membrane lipid peroxides and progressive lipid peroxidation.

This result supports our hypothesis that SPIONs induce ferroptosis. Moreover, the protective agents α-tocopherol, ferrostatin-1 and OA effectively reversed the GPX4 down-regulation caused by RSL3 and SPIONs, further corroborating the ferroptotic nature of SPION-induced cell death.

Finally, our flow cytometry analyses of cellular plasma membrane integrity also revealed similarities between the mechanisms of RSL3- and SPION-induced cell death pointing to a common mechanism consistent with ferroptosis.

In previous studies, the effects of SPIONs (iron oxide nanoparticles (IONs) with a core size of 5 to 15 nm)[66] and other IONs on endothelial cells were investigated in detail. Their effects have been shown to vary widely depending on factors such as particle size, dose, core and coating composition, and experimental conditions.[67–70] However, given the relatively recent discovery of ferroptosis, the influence of IONs on ferroptosis in endothelial cells has not yet been sufficiently investigated. A study by Zhang et al[71] showed that the nuclear composition of SPIONs can significantly affect their ability to induce ferroptosis. They investigated the interactions of three different types of SPIONs with a core size of around 10 nm with HUVEC cells. Fe_2O_3 NPs coated with meso-2,3-dimercaptosuccinic acid (DMSA) caused cell death by both ferroptosis and apoptosis, while DMSA-Fe_3O_4 NPs primarily induced ferroptosis. Coating with polyglucose sorbitol carboxymethyl ether (PSC) inhibited cellular uptake of IONs, resulting in PSC-Fe_2O_3 NPs having no effect on cell viability. On the other hand, Liu et al[72] demonstrated that both γ-Fe_2O_3 NPs with a diameter of 55 nm and Fe_3O_4 NPs with a diameter of 14 nm induced ferroptosis in HUVEC cells. Despite slight differences in cytotoxicity and uptake efficiency between γ-Fe_2O_3 and Fe_3O_4 NPs, the results showed no mechanistic dissimilarity in the induction of ferroptosis by these two types of IONs.

Silica-Coated SPIONs Do Not Induce Apoptosis

To further investigate the effects of silica-coated SPIONs on cell membranes and to explore the possible involvement of apoptosis, we examined the distribution of phosphatidyl serine (PS) in the cell membrane and found no single positive cells in SPIONs-treated samples. PS is a phospholipid that is normally located on the inner leaflet of the plasma

membrane. Its exposure on the outer leaflet (in the absence of membrane rupture, which is detected by PI staining) is a hallmark of apoptosis and serves as a scavenger signal for phagocytes, indicating that the cell is dying and should be engulfed and eliminated.[73] Recently, many researchers have reported PS exposure also in non-apoptotic cells.[74] For example, PS exposure can also occur during ferroptosis[75] but it is not always as pronounced as in apoptosis.[76]

Our findings align with other studies indicating that SPIONs do not induce apoptosis in endothelial cells. Notably, some research suggests that SPIONs may even offer protective effects against apoptosis. For instance, Astanina et al[77] utilized Endorem, a dextran-stabilized SPION with a primary size of 5 nm, approved as an intravenous contrast agent. They exposed cells to the highest concentration of Endorem (2 mM) and incubated them with the nanoparticles for up to 3 days. Throughout all tested periods, Endorem exhibited neither pro-apoptotic activity nor cytotoxicity. Similarly, Catalano et al[78] synthesized Fe_3O_4 and silica-coated Fe_3O_4 SPIONs with diameters of approximately 10–15 nm. In vitro characterization demonstrated that both types of SPIONs are compatible with a mouse endothelial cell line, as confirmed by direct and indirect cytotoxicity assays, ROS generation, and the activation of apoptosis-related enzymes. Additionally, Duan et al[68] showed that SPIONs with an iron oxide core of about 5–10 nm and a dextran coating (Dex-SPIONs) can be internalized by HUVEC cells without causing significant cytotoxicity, while simultaneously inducing autophagy. Their results further indicate that Dex-SPIONs can enhance the survival of HUVEC cells and counteract H_2O_2-induced apoptosis.

Cell Morphology

Since ferroptosis is accompanied by membrane changes, such as cell blebbing and the formation of extracellular vesicles, scanning electron microscopy (SEM) may serve as a suitable alternative to TEM for studying and identifying such process.[79] SEM can also provide detailed information on the general shape and size of ferroptotic cells. To characterize the morphological changes associated with ferroptosis, we examined cells exposed to the ferroptosis inducer RSL3 using high-resolution SEM. We compared these changes with those observed in cells undergoing apoptosis (treated with staurosporine), unexposed cells, and cells treated with silica-coated SPIONs. We hypothesized that we would be able to distinguish between apoptotic and ferroptotic cells, and that cells treated with silica-coated SPIONs would exhibit morphological characteristics more similar to ferroptotic cells.

As expected, all three treatments (staurosporine, RSL3, and SPIONs) triggered cell death, characterized by lower cell density and more rounded, detached cells. Cell blebbing was observed in all treated groups but not in the untreated cells. Lamellipodia and filopodia were present in both treated and untreated cells.[54] Staurosporine uniquely induced a large number of unbranched, actin-based long cell extensions. These filopodia-like protrusions are not associated with apoptosis but are likely due to staurosporine interfering with cytoskeletal proteins, leading to changes in cell shape and migration.

Our results show that SEM images can effectively distinguish between the morphology of healthy, untreated cells and cells that have been triggered to undergo cell death by various agents (staurosporine, RSL3, SPIONs). However, the morphological changes observed in apoptosis and ferroptosis are remarkably similar and include decreased cell density, cell blebbing and an increased number of extracellular vesicles. Although SPION-exposed cells show more morphological similarities to RSL3-exposed cells than to staurosporine-exposed cells, this is primarily due to the unique morphological effects of staurosporine.[80] We note that staurosporine may not be the optimal trigger for apoptosis in studies focusing on morphological changes, as its specific effects may mask typical apoptotic features and potentially confound interpretations. All together these results suggests indeed that TEM is still the best method to study ferroptosis.

In fact, when viewed using TEM, treated cells exhibited several distinct characteristics of ferroptosis (Figure 7D–H),[59] such as dilated ER cisternae, several fragmented inner membranes, membrane blebs, which might be caused by lipid peroxidation, and presented swollen mitochondria with a reduced number of cristae and electron-lucent matrix.[81]

Ferroptosis is also known to induce autophagy, a catabolic process where cellular components are degraded and recycled. Such process was clearly visible in SPION-treated cells where we observed an increase in the number of autophagosomes which also contained multiple membrane structures, some of which resembled myelin, a type of membrane which mainly consists of plasmalogens.

Plasmalogens are a unique type of glycerophospholipid characterized by a vinyl-ether bond at the sn-1 position of the glycerol backbone, where an alkyl chain is attached. The sn-2 position typically carries a polyunsaturated fatty acid.[82]

Plasmalogens, are one of the major lipid components of the cell membranes where they play an important role in membrane organization and stability. They often accumulate in autophagic vacuoles as a result of lipid peroxidation. In this context, plasmalogens may also function and be considered as endogenous antioxidants, but they undergo oxidative decomposition due to oxidative stress more readily than other fatty acid ester analogues.[82–84]

Conclusion

This study demonstrates that silica-coated SPIONs induce ferroptosis via oxidative stress, lipid peroxidation, and GPX4 downregulation. Oleic acid (OA), a monounsaturated fatty acid, shows a promising protective effect by reducing particle-induced cell death and enhancing GPX4 expression, despite exerting a weaker impact on lipid peroxidation compared to classic ferroptosis inhibitors like ferrostatin-1 and α-tocopherol. OA's ability to counteract particle-induced ferroptosis may originate not only from its modulation of GPX4 expression but also from its capacity to replace PUFA in the plasma membrane, thereby reducing susceptibility to lipid peroxidation and membrane rupture. These findings align with our previous work (Repar et al, 2022)[35] and the one of Magtanong et al 2019,[36] providing deeper insight into the mechanisms underlying SPION-induced ferroptotic cell death and highlighting the potential role of oleic acid as an effective modulator of SPION-related side effects in cancer therapy.

However, it is important to highlight that this study has certain limitations. All experiments were conducted using a single cell line, which may not fully capture the variability of cellular responses to SPION exposure and oleic acid supplementation. Thus, additional experiments using other cell lines (eg Human Aortic Endothelial Cells (HAEC), Human Pulmonary Artery Endothelial Cells (HPAEC) etc.) are needed to determine whether the observed effects are broadly applicable or specific to the cell type used in this study. Moreover, a promising direction for future research would be to conduct time-course experiments to identify the "point of no return" beyond which oleic acid can no longer exert its antiferroptotic effects. This approach could provide valuable insights into the potency and temporal limits of oleic acid's protective action.

Data Sharing Statement

Data is available from the corresponding author upon reasonable request.

Acknowledgments

Funding

Disclosure

The authors confirm that they have no conflicts of interest to disclose in this work.

References

1. Dixon SJ, Lemberg KM, Lamprecht MR, et al. Ferroptosis: an iron-dependent form of nonapoptotic cell death. *Cell*. 2012;149(5):1060–1072. doi:10.1016/j.cell.2012.03.042
2. Berndt C, Alborzinia H, Amen VS, et al. Ferroptosis in health and disease. *Redox Biol*. 2024;75:103211. doi:10.1016/j.redox.2024.103211

3. Aldrovandi M, Fedorova M, Conrad M. Juggling with lipids, a game of Russian roulette. *Trends Endocrinol Metab*. 2021;32(7):463–473. doi:10.1016/j.tem.2021.04.012

4. Tang D, Chen X, Kang R, Kroemer G. Ferroptosis: molecular mechanisms and health implications. *Cell Res*. 2020;31(2):107–125. doi:10.1038/s41422-020-00441-1

5. Lei P, Bai T, Sun Y. Mechanisms of ferroptosis and relations with regulated cell death: a review. *Front Physiol*. 2019;10(FEB):1–13. doi:10.3389/fphys.2019.00139

6. Zhou Q, Meng Y, Li D, et al. Ferroptosis in cancer: from molecular mechanisms to therapeutic strategies. *Signal Transduct Target Ther*. 2024;9(1). doi:10.1038/s41392-024-01769-5

7. Yang WS, Stockwell Brent R. Synthetic lethal screening identifies compounds activating iron-dependent, nonapoptotic cell death in oncogenic-RAS-harboring cancer cells. *Chem Biol*. 2008;15(3):234–245. doi:10.1016/j.chembiol.2008.02.010.Synthetic

8. Elgendy SM, Alyammahi SK, Alhamad DW, Abdin SM, Omar HA. Ferroptosis: an emerging approach for targeting cancer stem cells and drug resistance. *Crit Rev Oncol Hematol*. 2020;155(June):103095. doi:10.1016/j.critrevonc.2020.103095

9. Zhang C, Liu X, Jin S, Chen Y, Guo R. Ferroptosis in cancer therapy: a novel approach to reversing drug resistance. *Mol Cancer*. 2022;21(1):47. doi:10.1186/s12943-022-01530-y

10. Wang HT, Ju J, Wang SC, et al. Insights Into ferroptosis, a novel target for the therapy of cancer. *Front Oncol*. 2022;12. doi:10.3389/fonc.2022.812534

11. Zaffaroni N, Beretta GL. Nanoparticles for ferroptosis therapy in cancer. *Pharmaceutics*. 2021;13(11). doi:10.3390/pharmaceutics13111785

12. Gong Y, Hu X, Chen M, Wang J. Recent progress of iron-based nanomaterials in gene delivery and tumor gene therapy. *J Nanobiotechnol*. 2024;22(1):309. doi:10.1186/s12951-024-02550-0

13. Huang G, Chen H, Dong Y, et al. Superparamagnetic iron oxide nanoparticles: amplifying ROS stress to improve anticancer drug efficacy. *Theranostics*. 2013;3(2):116. doi:10.7150/THNO.5411

14. Zhang Y, Hai Y, Miao Y, et al. The toxicity mechanism of different sized iron nanoparticles on human breast cancer (MCF7) cells. *Food Chem*. 2021;341(October 2020):128263. doi:10.1016/j.foodchem.2020.128263

15. Ni Z, Nie X, Zhang H, et al. Atranorin driven by nano materials SPION lead to ferroptosis of gastric cancer stem cells by weakening the mRNA 5-hydroxymethylcytidine modification of the Xc-/GPX4 axis and its expression. *Int J Med Sci*. 2022;19(11):1680–1694. doi:10.7150/IJMS.73701

16. Sang M, Luo R, Bai Y, et al. Mitochondrial membrane anchored photosensitive nano-device for lipid hydroperoxides burst and inducing ferroptosis to surmount therapy-resistant cancer. *Theranostics*. 2019;9(21):6209. doi:10.7150/THNO.36283

17. Chen M, Li J, Shu G, et al. Homogenous multifunctional microspheres induce ferroptosis to promote the anti-hepatocarcinoma effect of chemoembolization. *J Nanobiotechnol*. 2022;20(1):1–20. doi:10.1186/S12951-022-01385-X/FIGURES/7

18. Qi D, Peng M. Ferroptosis-mediated immune responses in cancer. *Front Immunol*. 2023;14(May):1–15. doi:10.3389/fimmu.2023.1188365

19. Doll S, Freitas FP, Shah R, et al. FSP1 is a glutathione-independent ferroptosis suppressor. *Nature*. 2019;575(7784):693–698. doi:10.1038/s41586-019-1707-0

20. Bai T, Li M, Liu Y, Qiao Z, Wang Z. Inhibition of ferroptosis alleviates atherosclerosis through attenuating lipid peroxidation and endothelial dysfunction in mouse aortic endothelial cell. *Free Radic Biol Med*. 2020;160(1):92–102. doi:10.1016/j.freeradbiomed.2020.07.026

21. Luo EF, Li HX, Qin YH, et al. Role of ferroptosis in the process of diabetes-induced endothelial dysfunction. *World J Diabetes*. 2021;12(2):124–137. doi:10.4239/wjd.v12.i2.124

22. Bin XH, Guo JH, Yang MM, Wang JT. Kinase PIM1 governs ferroptosis to reduce retinal microvascular endothelial cell dysfunction triggered by high glucose. *Vitro Cell Dev Biol Anim*. 2024;60(3):278–286. doi:10.1007/s11626-024-00882-7

23. Liu Z. Cardiac microvascular dysfunction and cardiomyopathy in diabetes: is ferroptosis a therapeutic target? *Diabetes*. 2023;72(3):313–315. doi:10.2337/dbi22-0036

24. Xie SS, Deng Y, lan GS, et al. Endothelial cell ferroptosis mediates monocrotaline-induced pulmonary hypertension in rats by modulating NLRP3 inflammasome activation. *Sci Rep*. 2022;12(1):1–16. doi:10.1038/s41598-022-06848-7

25. Zhang Y, Xin L, Xiang M, et al. The molecular mechanisms of ferroptosis and its role in cardiovascular disease. *Biomed Pharmacother*. 2022;145:112423. doi:10.1016/J.BIOPHA.2021.112423

26. Pucci C, Degl'Innocenti A, Belenli Gümüş M, Ciofani G. Superparamagnetic iron oxide nanoparticles for magnetic hyperthermia: recent advancements, molecular effects, and future directions in the omics era. *Biomater Sci*. 2022;10(9):2103–2121. doi:10.1039/d1bm01963e

27. Zheng H, Jiang J, Xu S, et al. Nanoparticle-induced ferroptosis: detection methods, mechanisms and applications. *Nanoscale*. 2021;13(4):2266–2285. doi:10.1039/D0NR08478F

28. Du S, Li J, Du C, Huang Z, Chen G, Yan W. Overendocytosis of superparamagnetic iron oxide particles increases apoptosis and triggers autophagic cell death in human osteosarcoma cell under a spinning magnetic field. *Oncotarget*. 2017;8(6):9410–9424. doi:10.18632/oncotarget.14114

29. Shen Y, Gong S, Li J, et al. Co-loading antioxidant N-acetylcysteine attenuates cytotoxicity of iron oxide nanoparticles in hypoxia/ reoxygenation cardiomyocytes. *Int J Nanomed*. 2019;14:6103–6115. doi:10.2147/IJN.S209820

30. Marekova D, Turnovcova K, Sursal TH, Gandhi CD, Jendelova P, Jhanwar-Uniyal M. Potential for treatment of glioblastoma: new aspects of superparamagnetic iron oxide nanoparticles. *Anticancer Res*. 2020;40(11):5989–5994. doi:10.21873/anticanres.14619

31. Jin R, Liu L, Zhu W, et al. Iron oxide nanoparticles promote macrophage autophagy and inflammatory response through activation of toll-like Receptor-4 signaling. *Biomaterials*. 2019;203(February):23–30. doi:10.1016/j.biomaterials.2019.02.026

32. Wu Y, Li L, Ning Z, et al. Autophagy-modulating biomaterials: multifunctional weapons to promote tissue regeneration. *Cell Commun Signaling*. 2024;22(1):1–39. doi:10.1186/s12964-023-01346-3

33. Liu L, Sha R, Yang L, et al. Impact of morphology on iron oxide nanoparticles-induced inflammasome activation in macrophages. *ACS Appl Mater Interfaces*. 2018;10(48):41197–41206. doi:10.1021/acsami.8b17474

34. Liu Y, Li J, Xu K, et al. Characterization of superparamagnetic iron oxide nanoparticle-induced apoptosis in PC12 cells and mouse hippocampus and striatum. *Toxicol Lett*. 2018;292(November 2017):151–161. doi:10.1016/j.toxlet.2018.04.033

35. Repar N, Jovičić EJ, Kump A, et al. Oleic acid protects endothelial cells from silica-coated superparamagnetic iron oxide nanoparticles (SPIONs)-induced oxidative stress and cell death. *Int J Mol Sci*. 2022;23(13):6972. doi:10.3390/ijms23136972

36. Magtanong L, Ko PJ, To M, et al. Exogenous monounsaturated fatty acids promote a ferroptosis-resistant cell state. *Cell Chem Biol*. 2019;26(3):420–432.e9. doi:10.1016/j.chembiol.2018.11.016

15457

37. Kralj S, Makovec D, Čampelj S, Drofenik M. Producing ultra-thin silica coatings on iron-oxide nanoparticles to improve their surface reactivity. *J Magn Magn Mater*. 2010;322(13):1847–1853. doi:10.1016/J.JMMM.2009.12.038

38. Kralj S, Makovec D. The chemically directed assembly of nanoparticle clusters from superparamagnetic iron-oxide nanoparticles. *RSC Adv*. 2014;4 (25):13167–13171. doi:10.1039/C4RA00776J

39. Kralj S, Makovec D. Magnetic assembly of superparamagnetic iron oxide nanoparticle clusters into nanochains and nanobundles. *ACS Nano*. 2015;9(10):9700–9707. doi:10.1021/ACSNANO.5B02328/SUPPL_FILE/NN5B02328_SI_001.PDF

40. Kralj S, Longobardo F, Iglesias D, et al. Ex-solution synthesis of Sub-5-nm FeOx nanoparticles on mesoporous hollow N,O-doped carbon nanoshells for electrocatalytic oxygen reduction. *ACS Appl Nano Mater*. 2019;2(10):6092–6097. doi:10.1021/ACSANM.9B01511/SUPPL_FILE/AN9B01511_SI_001.PDF

41. Nemec S, Kralj S. A versatile interfacial coassembly method for fabrication of tunable silica shells with radially aligned dual mesopores on diverse magnetic core nanoparticles. *ACS Appl Mater Interfaces*. 2021;13(1):1883–1894. doi:10.1021/ACSAMI.0C17863/SUPPL_FILE/AM0C17863_SI_001.PDF

42. Kolosnjaj-Tabi J, Kralj S, Griseti E, et al. Magnetic silica-coated iron oxide nanochains as photothermal agents, disrupting the extracellular matrix, and eradicating cancer cells. *Cancers*. 2019;11(12):2040. doi:10.3390/CANCERS11122040

43. Tadic M, Lazovic J, Panjan M, Kralj S. Hierarchical iron oxide nanocomposite: bundle-like morphology, magnetic properties and potential biomedical application. *Ceram Int*. 2022;48(11):16015–16022. doi:10.1016/J.CERAMINT.2022.02.145

44. Tadic M, Kralj S, Jagodic M, Hanzel D, Makovec D. Magnetic properties of novel superparamagnetic iron oxide nanoclusters and their peculiarity under annealing treatment. *Appl Surf Sci*. 2014;322:255–264. doi:10.1016/J.APSUSC.2014.09.181

45. Jarc E, Kump A, Malavašič P, Eichmann TO, Zimmermann R, Petan T. Lipid droplets induced by secreted phospholipase A2 and unsaturated fatty acids protect breast cancer cells from nutrient and lipotoxic stress. *Biochim Biophys Acta Mol Cell Biol Lipids*. 2018;1863(3):247–265. doi:10.1016/j.bbalip.2017.12.006

46. Burattini S, Falcieri E. Analysis of cell death by electron microscopy. *Methods Mol Biol*. 2013;1004:77–89. doi:10.1007/978-1-62703-383-1_7/FIGURES/00072

47. Rello S, Stockert JC, Moreno V, A G. Morphological criteria to distinguish cell death induced by apoptotic and necrotic treatments. *Apoptosis*. 2005;10(1):201–208. doi:10.1007/s10495-005-6075-6

48. Khajah MA, Luqmani YA. Involvement of membrane blebbing in immunological disorders and cancer. *Med Princ Pract*. 2016;25(2):18–27. doi:10.1159/000441848

49. Yang C, Czech L, Gerboth S, Kojima SI, Scita G, Svitkina T. Novel roles of formin mDia2 in lamellipodia and filopodia formation in motile cells. *PLoS Biol*. 2007;5(11):e317. doi:10.1371/JOURNAL.PBIO.0050317

50. Sens P, Plastino J. Membrane tension and cytoskeleton organization in cell motility. *J Phys*. 2015;27(27):273103. doi:10.1088/0953-8984/27/27/273103

51. Rottner K, Faix J, Bogdan S, Linder S, Kerkhoff E. Actin assembly mechanisms at a glance. *J Cell Sci*. 2017;130(20):3427–3435. doi:10.1242/JCS.206433

52. Hoelzle MK, Svitkina T. The cytoskeletal mechanisms of cell-cell junction formation in endothelial cells. *Mol Biol Cell*. 2012;23(2). doi:10.1091/mbc.E11-08-0719

53. Svitkina T. The actin cytoskeleton and actin-based motility. *Cold Spring Harb Perspect Biol*. 2018;10(1). doi:10.1101/CSHPERSPECT.A018267

54. Zurzolo C. Tunneling nanotubes: reshaping connectivity. *Curr Opin Cell Biol*. 2021;71:139–147. doi:10.1016/J.CEB.2021.03.003

55. Ljubojevic N, Henderson JM, Zurzolo C. The Ways of Actin: why Tunneling Nanotubes Are Unique Cell Protrusions. *Trends Cell Biol*. 2021;31 (2):130–142. doi:10.1016/j.tcb.2020.11.008

56. Hurtig J, Chiu DT. Intercellular nanotubes: insights from imaging studies and beyond. *Wiley Interdiscip Rev Nanomed Nanobiotechnol*. 2017;4:1–29. doi:10.1002/wnan.80.Intercellular

57. Chen Z, Lin H, Wang X, et al. The application of approaches in detecting ferroptosis. *Heliyon*. 2024;10(1):e23507. doi:10.1016/J.HELIYON.2023.E23507

58. Li FJ, Long HZ, Zhou ZW, Luo HY, Xu SG, Gao LC. System Xc−/GSH/GPX4 axis: an important antioxidant system for the ferroptosis in drug-resistant solid tumor therapy. *Front Pharmacol*. 2022;13:910292. doi:10.3389/FPHAR.2022.910292/BIBTEX

59. Dietrich C, Hofmann TG. Ferroptosis meets cell–cell contacts. *Cells*. 2021;10(9):2462. doi:10.3390/CELLS10092462

60. Mann J, Reznik E, Santer M, et al. Ferroptosis inhibition by oleic acid mitigates iron-overload-induced injury. *Cell Chem Biol*. 2024;31(2):249–264.e7. doi:10.1016/j.chembiol.2023.10.012

61. Levada K, Pshenichnikov S, Omelyanchik A, et al. Progressive lysosomal membrane permeabilization induced by iron oxide nanoparticles drives hepatic cell autophagy and apoptosis. *Nano Converg*. 2020;7(1):17. doi:10.1186/s40580-020-00228-5

62. Ziglari T, Wang Z, Holian A. Contribution of particle-induced lysosomal membrane hyperpolarization to lysosomal membrane permeabilization. *Int J Mol Sci*. 2021;22(5):2277. doi:10.3390/ijms22052277

63. Skouta R, Dixon SJ, Wang J, et al. Ferrostatins inhibit oxidative lipid damage and cell death in diverse disease models. *J Am Chem Soc*. 2014;136 (12):4551–4556. doi:10.1021/ja411006a

64. Magtanong L, Ko PJ, Dixon SJ. Emerging roles for lipids in non-apoptotic cell death. *Cell Death Differ*. 2016;23(7):1099–1109. doi:10.1038/cdd.2016.25

65. Sui X, Zhang R, Liu S, et al. RSL3 drives ferroptosis through GPX4 inactivation and ros production in colorectal cancer. *Front Pharmacol*. 2018;9 (NOV):1–8. doi:10.3389/fphar.2018.01371

66. Dulińska-Litewka J, Łazarczyk A, Hałubiec P, Szafrański O, Karnas K, Karewicz A. Superparamagnetic iron oxide nanoparticles-current and prospective medical applications. *Materials*. 2019;12(4). doi:10.3390/ma12040617

67. Matuszak J, Dörfler P, Zaloga J, et al. Shell matters: magnetic targeting of SPIONs and in vitro effects on endothelial and monocytic cell function. *Clin Hemorheol Microcirc*. 2015;61(2):259–277. doi:10.3233/CH-151998

68. Duan J, Du J, Jin R, et al. Iron oxide nanoparticles promote vascular endothelial cells survival from oxidative stress by enhancement of autophagy. *Regen Biomater*. 2019. doi:10.1093/rb/rbz024

69. Mulens-Arias V, Rojas JM, Sanz-Ortega L, Portilla Y, Pérez-Yagüe S, Barber DF. Polyethylenimine-coated superparamagnetic iron oxide nanoparticles impair in vitro and in vivo angiogenesis. *Nanomedicine*. 2019. doi:10.1016/j.nano.2019.102063

70. Salingova B, Simara P, Matula P, et al. The effect of uncoated SPIONs on hiPSC-differentiated endothelial cells. *Int J Mol Sci*. 2019;20(14):1–16. doi:10.3390/ijms20143536

71. Zhang X, Kong F, Wang T, et al. Iron oxide nanoparticles cause surface coating- and core chemistry-dependent endothelial cell ferroptosis. *Nanotoxicology*. 2022;16(9–10):829–843. doi:10.1080/17435390.2022.2154176

72. Liu Z, Xia X, Lv X, Song E, Song Y. Iron-bearing nanoparticles trigger human umbilical vein endothelial cells ferroptotic responses by promoting intracellular iron level. *Environ Pollut*. 2021;287(May):117345. doi:10.1016/j.envpol.2021.117345

73. Nagata S, Suzuki J, Segawa K, Fujii T. Exposure of phosphatidylserine on the cell surface. *Cell Death Differ*. 2016;23(6):952–961. doi:10.1038/cdd.2016.7

74. Shlomovitz I, Speir M, Gerlic M. Flipping the dogma - Phosphatidylserine in non-apoptotic cell death. *Cell Commun Signaling*. 2019;17(1):1–12. doi:10.1186/s12964-019-0437-0

75. Klöditz K, Fadeel B. Three cell deaths and a funeral: macrophage clearance of cells undergoing distinct modes of cell death. *Cell Death Discov*. 2019;5(1). doi:10.1038/s41420-019-0146-x

76. Wiernicki B, Maschalidi S, Pinney J, et al. Cancer cells dying from ferroptosis impede dendritic cell-mediated anti-tumor immunity. *Nat Commun*. 2022;13(1):1–15. doi:10.1038/s41467-022-31218-2

77. Astanina K, Simon Y, Cavelius C, Petry S, Kraegeloh A, Kiemer AK. Superparamagnetic iron oxide nanoparticles impair endothelial integrity and inhibit nitric oxide production. *Acta Biomater*. 2014;10(11):4896–4911. doi:10.1016/j.actbio.2014.07.027

78. Catalano E, Miola M, Ferraris S, et al. Magnetite and silica-coated magnetite nanoparticles are highly biocompatible on endothelial cells in vitro. *Biomed Phys Eng Express*. 2017;3(2). doi:10.1088/2057-1976/aa62cc

79. Chen F, Kang R, Tang D, Liu J. Ferroptosis: principles and significance in health and disease. *J hematol oncol*. 2024;17(1):1–41. doi:10.1186/S13045-024-01564-3

80. Olguín-Albuerne M, Domínguez G, Morán J. Effect of staurosporine in the morphology and viability of cerebellar astrocytes: role of reactive oxygen species and NADPH oxidase. *Oxid Med Cell Longev*. 2014;2014. doi:10.1155/2014/678371

81. Chen X, Kang R, Kroemer G, Tang D. Organelle-specific regulation of ferroptosis. *Cell Death Differ*. 2021;28(10):2843–2856. doi:10.1038/s41418-021-00859-z

82. Paul S, Lancaster GI, Meikle PJ. Plasmalogens: a potential therapeutic target for neurodegenerative and cardiometabolic disease. *Prog Lipid Res*. 2019;74:186–195. doi:10.1016/j.plipres.2019.04.003

83. Brites P, Waterham HR, Wanders RJA. Functions and biosynthesis of plasmalogens in health and disease. *Biochimica et Biophysica Acta*. 2004;1636(2–3):219–231. doi:10.1016/j.bbalip.2003.12.010

84. Broniec A, Klosinski R, Pawlak A, Wrona-Krol M, Thompson D, Sarna T. Interactions of plasmalogens and their diacyl analogs with singlet oxygen in selected model systems. *Free Radic Biol Med*. 2011;50(7):892–898. doi:10.1016/j.freeradbiomed.2011.01.002